

---

---

CLASSICAL PROBLEMS OF LINEAR ACOUSTICS  
AND WAVE THEORY

---

---

## Determination of the Elastic Properties of a Solid Sphere Based on the Results of Acoustic Beam Scattering

L. M. Kotelnikova<sup>a,\*</sup>, D. A. Nikolaev<sup>a</sup>, S. A. Tsysar<sup>a</sup>, and O. A. Sapozhnikov<sup>a</sup>

<sup>a</sup> *Moscow State University, Physics Faculty, Moscow, 119991 Russia*

\**e-mail: kotelnikova.lm16@physics.msu.ru*

Received December 26, 2020; revised April 16, 2021; accepted April 23, 2021

**Abstract**—When using elastic spherical scatterers in acoustic problems, it is necessary to know their main elastic parameters that characterize the internal resonances. In this study, it has been shown that the velocities of longitudinal and transverse waves in a solid sphere can be determined from the scattering characteristics of an ultrasound beam. Millimeter-sized steel, glass, and nylon spheres that were immersed in water were considered as scatterers. In experiments an acoustic field was created by a flat piezoelectric source operating in the megahertz frequency range in a pulsed mode. By comparing the experimental data and numerical calculations for the scattered-field amplitude, the velocities of elastic waves in the materials of spheres were determined and their absorption coefficients were estimated.

**Keywords:** scattering of acoustic waves, elastic scatterer, experiment

**DOI:** 10.1134/S1063771021040072

### 1. INTRODUCTION

When a wave field interacts with a body of a finite size, the characteristics of a scattered wave are determined not only by the dimensions and shape of this body but also by its acoustic parameters [1–5]. In practice, these parameters are often unknown or specified with a low accuracy, thus making it impossible to quantitatively analyze the phenomena that depend on spatiotemporal characteristics of scattered waves. Such phenomena include, e.g., the effect of the acoustic radiation force [6].

The theoretical analysis of the acoustic radiation force that acts on an elastic body is based on the solution of the scattering problem. For this purpose, it is important to know the main parameters of the scatterer used in experiments, which characterize the internal resonances, such as the size, density, and the velocities of longitudinal and transverse waves. When considering an elastic scatterer, its geometric characteristics can be measured directly, the density can be calculated, if the volume and mass, which is found via weighing, are known, while the velocities of elastic waves in a small scatterer cannot be measured easily. These velocities depend not only on the chemical composition but also on the internal structure, which is defined by the manufacturing technique and processing procedures; therefore, these values may vary for objects having the same composition but taken from different batches [7, 8]. As a result, the values of the elastic moduli specified by a manufacturer (which

actually determine the wave velocities) may be inconsistent with actual values.

Elastic objects are transparent to sound to a certain degree. In particular, acoustic waves incident on a spherical scatterer (sphere) excite internal vibrations in it, which make a significant contribution to the form of the scattered field. This can be observed in the angular distribution of the amplitude and total dissipated energy [9, 10]. These vibrations are related to the resonance phenomena inside the scatterer caused by both bulk and surface waves (Franz and Rayleigh waves and whispering-gallery modes) [11–20]. Since these phenomena depend on the physical properties of the scatterer, studying the features of scattering can be used to experimentally determine the unknown elastic velocities.

There exist many methods for calculating the acoustic scattering by an elastic sphere. In the approximation of incidence of a plane wave on a nonabsorbing sphere, there is an exact solution in the form of an infinite series of waves diverging from a scatterer and described by spherical harmonics. The features of the solution for this description were studied and confirmed experimentally in a number of papers [9, 10, 16, 21]. This approach can be used for calculating the scattering by spherical objects of relatively small dimensions, for  $ka < 100$ , where  $k$  is the wave number, and  $a$  is the radius of the sphere. Since rounding errors in the calculation of special functions become significant for large values of  $ka$  and the required number of terms of the corresponding series becomes large, the

accuracy decreases and the time spent on calculations increases significantly. In addition, although this approach makes it fairly easy to describe scattering, it does not provide a physical interpretation of the features of the resulting scattered field. This interpretation is provided by other calculation methods, e.g., the approach based on the Watson–Sommerfeld transform, which allows one to calculate scattering of waves at  $ka > 30$  [12, 22], or the method based on the theory of resonant acoustic scattering [11, 13, 15].

Previously, methods were proposed for determining unknown velocities of elastic waves in spheres immersed in a fluid based on the results of measuring the backscattering of a plane wave [8, 23–27]. Basically, these methods were designed to determine the elastic parameters of spheres used for calibration of hydroacoustic equipment; therefore, in the above studies, their diameters ranged from 20 to 90 mm for frequencies of up to 300 kHz. A sphere was placed in the far field of a source, and calculations were performed in the approximation of a plane wave incident on the scatterer. The use of this approximation was stated as one of the reasons for some amplitude deviations of the experiment from the theory. The measured scattered-field signal was much higher than the noise level, thus making it possible to analyze fine details of the scattered-wave spectrum. However, as the size of the scatterer decreases, the scattered-field signal will inevitably become weaker; therefore, for millimeter-sized spheres of practical interest, such methods may be inaccurate.

In [28], the possibility of studying the scattered field in the propagation direction of an incident wave was shown. This approach is used in our study to determine the velocities of elastic waves inside scatterers. The use of this method is convenient for the formulated purposes due to the relatively simple manipulations from the standpoint of alignment (for placing the scatterer on the acoustic axis of the source) and the ability to measure the acoustic field near a scatterer without introducing distortions into the structure of the incident wave.

As mentioned above, calculating the parameters in the plane wave approximation reduces the accuracy of determining the velocities of elastic waves in the scatterer material. This is caused by the fact that when actual sources are used, the acoustic field incident on the scatterer significantly differs from a plane wave in most cases. To increase the calculation accuracy, it is necessary to take the inhomogeneous spatial structure of the incident wave into account; this can be done proceeding either from the model assumption on the structure of surface vibrations of the used source (e.g., the assumption of the piston character of source vibrations), which also limits the accuracy, or, if possible, by using the acoustic holography method [29].

In this study, we have proposed a method for determining the velocities and absorption coefficients of

longitudinal and transverse waves in millimeter-sized solid-state spherical objects based on measuring the scattering characteristics of an ultrasound beam, i.e., the frequency dependence of the forward-scattering amplitude and the angular scattered-field distribution. An experimental setup for observing scattering by spheres is described. The unknown velocities and absorption coefficients are determined by comparing the experimental results and results of a numerical simulation, which was maximally close to the experimental conditions.

## 2. THEORETICAL METHODS

### 2.1. Description of Scattering of a Plane Wave by an Elastic Sphere

Before considering the case of a complex actual field structure of a wave incident on a scatterer, let us analyze the scattering process of an idealized plane acoustic wave. An isotropic elastic sphere, inside which both longitudinal and transverse waves are generally excited and which is immersed in an ideal fluid, is considered as the scatterer. A solution of such a problem was first presented in [9]. Let us present the statement and results of solving the scattering problem, which are necessary for the further consideration, using the designations introduced in [30].

Let a monochromatic plane wave be incident on an elastic sphere with radius  $a$ :

$$p_i = p_0 e^{ikz} = p_0 e^{ikr \cos \theta}, \quad (1)$$

where  $p_0$  is the complex amplitude of the incident wave;  $k = \omega/c = 2\pi f/c$  is the wave number;  $c$  is the sound velocity in the immersion fluid;  $z$  is the distance along the propagation direction of the incident wave;  $r$ ,  $\theta$ , and  $\varphi$  are the spherical coordinates (due to the symmetry of the problem, there is no dependence on the azimuthal angle  $\varphi$ ), the origin coincides with the center of the sphere; the angle  $\theta = 0^\circ$  corresponds to the wave propagation direction; and  $z = r \cos \theta$  (Fig. 1).

The wave field on the scatterer surface is described using the following appropriate boundary conditions: (1) the pressure in the fluid taken with an opposite sign is equal to the normal components of the stress in the scatterer; (2) the tangential components of transverse stresses in the scatterer are equal to zero; (3) the normal component of the vibrational velocity does not change upon a transition through the boundary.

Taking into account that the incident plane wave can be represented as an expansion into an infinite series with separation of the functions of the angular and radial variables [31]:

$$p_i = p_0 e^{ikr \cos \theta} = \sum_{n=0}^{\infty} p_0 i^n (2n+1) j_n(kr) P_n(\cos \theta), \quad (2)$$

it is convenient to seek the solution of the formulated problem for the acoustic pressure of the scattered field

in the form of a similar expansion. The choice of a spherical function describing the dependence of the solution on the distance is determined by the radiation condition with selection of only diverging waves from the scatterer:

$$p_s = \sum_{n=0}^{\infty} p_0 i^n (2n + 1) c_n h_n^{(1)}(kr) P_n(\cos\theta). \quad (3)$$

Here,  $P_n(\cos\theta)$  are the Legendre polynomials and  $h_n^{(1)}(\xi) = j_n(\xi) + in_n(\xi)$  is the spherical Hankel function of the first kind, where  $j_n(\xi)$  and  $n_n(\xi)$  are Bessel and Neumann spherical functions, respectively. The terms of the series that were found from the above boundary conditions have the following coefficients:

$$c_n = -\frac{\Gamma_n j_n(ka) - ka j_n'(ka)}{\Gamma_n h_n^{(1)}(ka) - ka h_n^{(1)'}(ka)}, \quad (4)$$

where the prime means the derivative with respect to the full argument of the corresponding functions. The values of  $c_n$  characterize the scattering and depend on the known properties of the immersion fluid and the material of the sphere, namely, on the velocity of sound  $c$  and density of the fluid, the sphere material density, as well as on the combinations  $k_1 a$ ,  $k_2 a$ , where  $k_l = \omega/c_l$ ,  $k_t = \omega/c_t$ , and  $c_l$  and  $c_t$  are the velocities of the longitudinal and transverse waves in the scatterer, respectively. The coefficients  $\Gamma_n$  depend only on the combinations  $k_1 a$ ,  $k_2 a$ , and the densities of the sphere  $\rho_*$  and fluid  $\rho$ :

$$\Gamma_n = \frac{\rho k_t^2 a^2 \alpha_n \delta_n + \beta_n \chi_n}{2\rho_* \alpha_n \eta_n + \beta_n \varepsilon_n}, \quad (5)$$

where

$$\begin{aligned} \alpha_n &= j_n(k_1 a) - k_1 a j_n'(k_1 a), \\ \delta_n &= 2n(n+1) j_n(k_1 a), \quad \beta_n = (n^2 + n - 2) j_n(k_1 a) + \\ &k_1^2 a^2 j_n''(k_1 a), \quad \chi_n = k_1 a j_n'(k_1 a), \quad \eta_n = 2n(n+1) \times \\ &[j_n(k_1 a) - k_1 a j_n'(k_1 a)], \\ \varepsilon_n &= k_1^2 a^2 [j_n(k_1 a) \sigma / (1 - 2\sigma) - j_n''(k_1 a)]. \end{aligned}$$

The scattering cross-section defined as  $\Sigma_s = W_s / I_i$ , where  $W_s$  is the scattered wave power and  $I_i$  is the incident wave intensity, is an important characteristic of scattering. In view of the asymptotics of the Hankel spherical function at large values of the argument  $h_n^{(1)}(z) \approx (-i)^{n+1} e^{iz} / z$ , using the optical theorem [21], and taking the expression for the scattered field (3) into consideration, we can derive the following expression for the scattering cross-section normalized by the cross-sectional area  $\pi a^2$ :

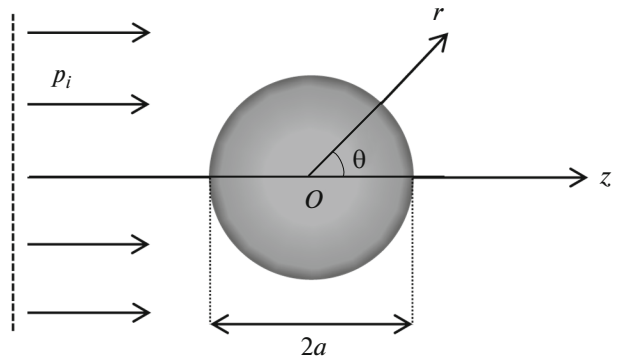


Fig. 1. Incidence of plane wave on sphere. Coordinate system.

$$\frac{\Sigma_s}{\pi a^2} = -\frac{4}{k^2 a^2} \sum_{n=0}^{\infty} (2n + 1) \text{Re}(c_n). \quad (6)$$

The dependence of the scattering cross-section on the frequency  $f = \omega/(2\pi)$  or parameter  $ka = 2\pi fa/c$  reflects the general character of the scattered-field behavior with an increase in the frequency, while the presence of peaks and dips in the dependence indicates the presence of resonance phenomena inside the sphere, which affect the form of the scattered field. The scattering cross-section depends on the density of the sphere material, the velocity of sound in water, and the velocities of longitudinal  $c_l$  and transverse  $c_t$  waves.

Numerical calculations of the scattered field and scattering cross-section for estimates of the scatterers used in the experiments were performed using formulas (3)–(6) in the MATLAB environment, which contains a large number of built-in functions, in particular, those for calculating Legendre polynomials and Bessel and Neumann functions. The spherical Bessel and Neumann functions  $j_n(\xi)$  and  $n_n(\xi)$ , respectively, were calculated according to the definitions  $j_n(\xi) = \sqrt{\pi/(2\xi)} J_{n+1/2}(\xi)$ ,  $n_n(\xi) = \sqrt{\pi/(2\xi)} N_{n+1/2}(\xi)$ , where  $J_n(\xi)$ ,  $N_n(\xi)$  are the Bessel and Neumann functions, respectively. The number of terms of the infinite series that was used in the calculations with formulas (3) and (6) was  $N_{\max} = (3-5)ka$ , which was sufficient for the convergence [32].

### 2.2. Accounting for Absorption in the Scatterer Material

It is known that when acoustic waves are scattered by metal spheres, the absorption at low frequencies is negligible and, therefore, it can be disregarded in calculations. However, this is not always the case for other materials. It is convenient to take the absorption in the scatterer material into account by introducing

imaginary parts into the wave numbers for longitudinal and transverse waves [33–35]:

$$\begin{aligned} k_l &= \frac{\omega}{c_l} + i\alpha_l = \frac{\omega}{c_l}(1 + i\tan\delta_l), \\ k_t &= \frac{\omega}{c_t} + i\alpha_t = \frac{\omega}{c_t}(1 + i\tan\delta_t), \end{aligned} \quad (7)$$

where  $\alpha_l, \alpha_t$  are the absorption coefficients, and  $\tan\delta_l, \tan\delta_t$  are the loss tangents for longitudinal and transverse waves, respectively.

The wave numbers  $k_l$  and  $k_t$  are included in the arguments of the spherical Bessel functions and their derivatives, which appear in the definition of the coefficients  $\Gamma_n$ . With the above modification of the wave numbers, these arguments become complex. Since MATLAB allows finding the values of the Bessel functions (through which spherical Bessel functions are expressed) for complex arguments, it is easy to calculate scattering with consideration for the absorption.

### 2.3. Scattering of an Ultrasound Beam by an Elastic Sphere

There are no infinitely extended sound sources able to generate a plane wave. All physically realizable acoustic sources produce limited sound beams. Therefore, in practice, the amplitude of a wave incident on the surface of a scatterer is different at different points, and the wave front differs from a plane front. If the wave incident on the scatterer does not differ much from a plane wave, it is then possible to continue using the plane-wave theory to calculate the scattered field with certain reservations; however, as the wave inhomogeneity increases, this approximation becomes less efficient, thus leading to a loss of some information about the parameters of the scatterer, which could be determined from the measured amplitude. In connection with this, it becomes necessary to take the spatial structure of the beam incident on the scatterer into account in order to increase the accuracy of determining the unknown parameters of the scatterer in theoretical calculations.

In this study, a numerical calculation of the scattered field caused by the incidence of an acoustic beam on an elastic sphere was performed on the basis of the theoretical approach described in [30].

Let a monochromatic wave beam be incident on an elastic sphere of radius  $a$ . Since any wave beam can be represented as a superposition of plane waves of different directions and the solution of the scattering problem is known for each of these plane waves, the solution for the scattered wave is generally represented as a superposition of expressions of the form of (3). This solution is transformed to a more compact form when using the addition theorem for spherical harmonics, which makes it possible to represent the complex amplitude of the acoustic pressure in the scattered

field as the following expansion into a series in terms of spherical harmonics [30]:

$$P_s = \sum_{n=0}^{\infty} \sum_{m=-n}^n s_{nm} h_n^{(1)}(kr) Y_{nm}(\theta, \varphi). \quad (8)$$

Here,  $Y_{nm}(\theta, \varphi)$  are spherical harmonics. The expansion coefficients  $s_{nm}$  are represented as  $s_{nm} = i^n c_n H_{nm} / \pi$ , where the expression for the coefficients  $c_n$  was determined earlier (formula (4)), while  $H_{nm} = \iint_{k_x^2 + k_y^2 \leq k^2} dk_x dk_y S(k_x, k_y) Y_{nm}^*(\theta_k, \varphi_k)$  are the coefficients that fully specify the incident field, which is characterized by the angular spectrum  $S(k_x, k_y)$ . The expressions for the angles  $\theta_k$  and  $\varphi_k$  are presented in [30]. The angular spectrum of the beam can be found from the formula:

$$S(k_x, k_y) = \int_{-\infty}^{+\infty} \int_{-\infty}^{+\infty} dx dy P(x, y, z_H) e^{-ik_x x - ik_y y}, \quad (9)$$

where  $P(x, y, z_H)$  is the complex amplitude of the acoustic pressure in the transverse plane that runs through the sphere center at the distance  $z_H$  from the source. This distribution can be found experimentally or be calculated using the Rayleigh integral with the known character of vibrations of the source surface [29]:

$$P(\mathbf{r}) = -\frac{ikc\rho}{2\pi} \int \frac{V_n(x', y', 0) e^{ikR}}{R} dx' dy', \quad (10)$$

where  $V_n(x', y', 0)$  is the particle velocity on the source surface,  $R = |\mathbf{r} - \mathbf{r}'|$ ,  $\mathbf{r}' = (x', y', 0)$ , and the integration is performed over the source surface. In the case of a circular piston source,  $V_n(\mathbf{r}') \equiv V_0 = \text{const}$  for  $x'^2 + y'^2 \leq a_{\text{rad}}^2$ ,  $V_n(\mathbf{r}') \equiv 0$  for  $x'^2 + y'^2 > a_{\text{rad}}^2$ , and  $a_{\text{rad}}$  is the source radius.

## 3. EXPERIMENT

### 3.1. Experimental Setup

Figure 2a schematically shows the experimental setup. A flat piezoceramic broadband source with a diameter of 38 mm (V392, Olympus, USA) with a center frequency of 1 MHz was placed in a tank with degassed water. A pulsed signal consisting of three periods of a sinusoidal signal was fed to the source from the generator. The center frequencies of the pulses used in the experiments for different scatterers are shown in Table 1. Due to the short duration of the emitted signal, it was possible to study the scattered field in a quite wide frequency band. The acoustic signal was measured using a capsule-type hydrophone (Onda HGL-0200, USA) with a sensing element diameter of 200  $\mu\text{m}$ . During the acoustic field scan-

ning, the hydrophone was moved by a micropositioning system (UMS-3, Precision Acoustics, UK) along three mutually perpendicular axes. The scatterer was mounted using a system of stretched fishing lines, which fixed the sphere at a certain distance from the source during measurements (Fig. 2b), and the small diameter of the lines ( $35.7\ \mu\text{m}$ ) allowed us not to take their influence on the acoustic field into account. Berkley NanoFil (Pure Fishing, Inc., USA) fishing lines were used, which are a hybrid of a braided cord and a monofilament fishing line.

The experiments used spheres made of grade AISI 440-C stainless steel with diameters of  $d = 2.8\text{--}6\ \text{mm}$ , glass (sodium–calcium–silicate glass, i.e., crystal glass) with diameters of  $d = 4\text{--}8\ \text{mm}$  and nylon (polyamide 6.6) with diameters of  $d = 4\text{--}8\ \text{mm}$ , which were placed at a distance of 350 mm from the source on its acoustic axis. The diameters were measured with a micrometer with a division value of 0.01 mm. The mass of a sphere was measured with an electronic balance with an accuracy of 0.001 g. Knowledge of the mass and diameter of the sphere allowed calculation of its density. The density measurement error in the end was 0.2–1.8% (see Table 1). The variation of the densities within the specified errors did not affect the value of the scattered field. Table 1 also shows the values of the steel, glass, and nylon densities based on the reference data [36–39].

The metal frame has a U-shaped structure consisting of two 20-cm-long vertical rods of circular cross section, which were spaced 20 cm apart and attached with their upper ends to a horizontally positioned rectangular rod (see Fig. 2a). Near the lower ends of the rods, there were drilled holes into which small inserts were placed that contained holes with a smaller diameter for threading and securing fishing lines. Four fishing lines were used, which were stretched in the gap between the rods. These lines were spaced so that due to the produced tension, it was possible to fix a sphere steadily between them (see Fig. 2b).

When waves were scattered by a sphere that was fixed between the fishing lines, the metal frame was beyond the region of the probing acoustic beam, thus making it possible to avoid parasitic scattering of the incident field by the frame.

At a certain distance from the center of the sphere, at which, according to calculations, the scattered field was comparable in magnitude to the incident field, the acoustic-pressure profiles were measured along the vertical  $y$  axis that passed through the acoustic axis, from which the amplitude and phase were determined. The distance was selected so that the signal from the scattered field was strong enough to minimize the influence of noise. The distance from the center of the sphere to the hydrophone at the central measurement point, which lies on the acoustic axis of the source, as well as other parameters, are shown in Table 1. During the experiment, a thermometer was used to measure

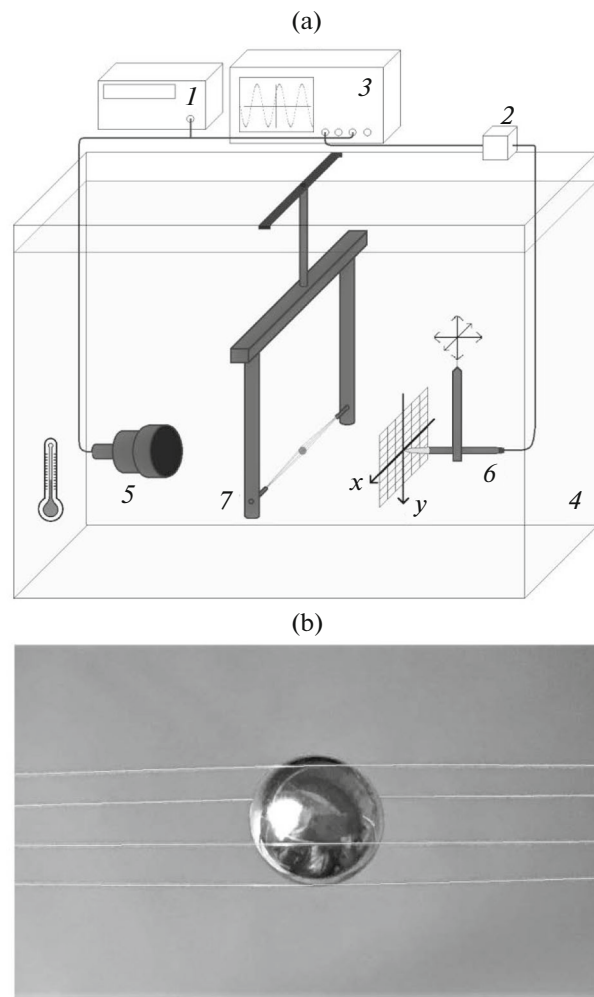


**Fig. 2.** (a) Diagram of experimental setup: (1) generator, (2) preamplifier, (3) oscilloscope, (4) water-filled tank, (5) source, (6) hydrophone, (7) metal frame with stretched fishing lines; (b) attachment of scatterer with a system of stretched fishing lines.

the water temperature, which was  $22.0 \pm 0.1^\circ\text{C}$  and did not change during the measurements.

### 3.2. Measurement and Experimental Data

#### Processing Methods

The experimental data processing and numerical calculations of the scattered field were carried out in the MATLAB environment.

The frequency dependences of the scattering cross-sections were calculated according to formula (6) for the spheres that were used in the experiment; the following values of the velocities of the longitudinal  $c_l$  and transverse  $c_t$  waves in the scatterer were taken in the calculation: for steel,  $c_l = 5900\ \text{m/s}$  and  $c_t = 3340\ \text{m/s}$ ; for glass,  $c_l = 5920\ \text{m/s}$  and  $c_t = 3420\ \text{m/s}$ ; for nylon,  $c_l = 2620\ \text{m/s}$  and  $c_t = 1080\ \text{m/s}$  (these values were

**Table 1.** Characteristics of scatterers and the input parameters

Sphere material	Sphere diameter $d$ , mm	Density $\rho$ , kg/m <sup>3</sup>	Density from reference data, kg/m <sup>3</sup>	Distance from the sphere center to the hydrophone $x$ , mm	Center frequency of a pulse, MHz
Steel	$2.763 \pm 0.005$	$7480 \pm 60$	7500–8200	20.2	1.0
	$4.744 \pm 0.005$	$7490 \pm 24$		35.3	0.85
	$5.989 \pm 0.005$	$7710 \pm 18$		59.7	1.1
Glass	$3.967 \pm 0.006$	$2552 \pm 23$	2240–2800	23.1	1.0
	$6.10 \pm 0.02$	$2653 \pm 26$		34.4	0.9
	$7.981 \pm 0.006$	$2477 \pm 6$		49.2	1.1
Nylon	$3.945 \pm 0.005$	$1104 \pm 20$	1020–1130	19.5	1.1
	$5.930 \pm 0.007$	$1088 \pm 7$		39.1	1.0
	$5.958 \pm 0.007$	$1074 \pm 6$		39.1	1.0
	$7.990 \pm 0.007$	$1119 \pm 6$		58.69	1.0

provided by the manufacturer of spheres, RGPBALLS SRL, Italy). To refine the specified values of  $c_l$  and  $c_t$ , proceeding from the obtained frequency dependences of the scattering cross-section, a frequency range was selected for each sphere that contained resonance regions sensitive to small changes in the elastic velocities. For the experiment, a short-duration pulse was used, whose spectrum covered the frequency range selected for this sphere, while the pulse carrier frequency corresponded to the central point of the range (see Table 1).

At a distance of 350 mm from the source, the central point of the recorded axially symmetric two-dimensional distribution of the wave amplitude was found by scanning the field in the transverse plane. It was considered as the point of the acoustic axis into which the center of the studied scatterer should be placed. For this purpose, after the end of scanning, the hydrophone was first moved to the found axial point of the scan segment and then moved several millimeters away from the source. Next, the frame with a sphere fixed between the stretched fishing lines was immersed into the tank so that the center of the sphere was directly in front of the sensitive area of the hydrophone. In this way, the sphere was placed on the acoustic axis of the source at a specified distance from it with an accuracy better than 1 mm. As follows from the calculations, the amplitude of the scattered field upon a displacement of the sphere by 1 mm in the transverse direction from the acoustic axis changes in magnitude at the point of the signal maximum by at most 2% (depending on the chosen sphere and frequency) relative to the amplitude for the symmetric arrangement of the sphere in the source field. It can also be assumed that the positions of the characteristic minima and maxima in the frequency response are not affected by such a shift. In this case, the accuracy of placing the source on the acoustic axis was better than 1 mm; thus, it can be assumed that a small possible

deviation of the sphere from the axis did not affect the measurement result.

The distance from the sphere to the source  $x_1$  was found by measuring the time within which a signal passed the distance from the source to the sphere and back after its reflection from the sphere surface that was closer to the source.

After the sphere was fixed in the desired position, in the presence of the sphere, a point with the maximum amplitude, where it was planned to measure the scattered field, was found (for a symmetrical position of the scatterer in the source field, this point lies on the acoustic axis) by scanning the field in the transverse plane at some distance from its center. The found point became the central point in the subsequent measurements of the scattered field on the  $y$  axis. The distance from this point to the source  $x_2$  was determined later, after the removal of the sphere, by measuring the delay time of the arrival of the emitted signal at the hydrophone. The distance  $x$  from the center of the sphere to the hydrophone was found from the formula  $x = x_2 - x_1 - d/2$  (see Table 1).

For each sphere at a fixed distance  $x_2$  from the source along the vertical  $y$  axis (across the acoustic axis of the source), the acoustic field was measured in the presence of the sphere (the full field) and in its absence (the incident field). By subtracting the complex amplitudes of the full and incident fields, the complex amplitude of the scattered wave was found, which, after being normalized to the amplitude of the incident field at the center of the sphere, was used for theoretical analysis. The amplitude of the incident field at the center of the sphere, on the one hand, can be measured with a hydrophone. On the other hand, knowledge of the incident-field amplitude at the central point of measurements (for convenience), the frequency corresponding to this amplitude, and the source diameter allows one to calculate the amplitude

of the source field at the sphere location, using the Rayleigh integral. A comparison of the amplitudes calculated in this way at the sphere location with the experimentally measured amplitudes shows a good coincidence. The relative discrepancy at the considered frequencies did not exceed 1%; therefore, this method for finding the field amplitude at the sphere location can be used to reduce the number of measurements and the time of the experiment, which is important to ensure the constancy of the external conditions for the experiment.

To test the effect of temperature variations during measurements, the incident-field signals were measured at the same point at different instants of time, which were separated by a time interval of 10–15 min, which corresponded to the time between successive measurements of the full and incident fields. There were no signal-phase shifts during this interval, thus indicating the constancy of the velocity of sound in water with time and, consequently, the temperature constancy.

It was checked independently that the attachment does not affect the resulting scattered field. The incident field of the source was measured in the presence of the metal frame and the system of fishing lines without a sphere and in the absence of a frame. It has been shown that the above signals, as well as their spectral amplitudes and phases, coincide; that is, the frame and fishing lines do not contribute to the scattered field and their presence can be disregarded. Another effect that could be caused by the fasteners is the damping of the scatterer vibrations (attenuation of surface waves) at the point of the contact between the spheres and fixing lines, which might cause a change in the shapes of the experimental resonance curves in comparison to those calculated theoretically. However, such an effect of the fishing lines was not observed in the analysis of the results of scattering; i.e., the lines were quite thin and, therefore, their contact area with the scatterer was too small to significantly affect it.

The sampling period of hydrophone signals was 8 ns, while the time window width was 100  $\mu$ s. The absence of waves that were rereflected from the walls of the tank or source was checked by increasing the pulse repetition frequency until rereflected signals began to appear on the oscilloscope screen; after this, the pulse repetition frequency was reduced to eliminate such overlaps. When processing within the 100- $\mu$ s window, a narrower window was selected for localizing the main pulse. This made it possible to eliminate the contribution from rereflections between the sphere and hydrophone and inside the hydrophone, as well as to reduce the noise that occurs during measurements. At the same time, the selected window was long enough to register a scattered-field signal for as long time as possible, whose tail stretches behind the main signal for some time and contains contributions from

the waves excited in the scatterer and reemitted into the fluid. This tail of the scattered signal is important for the appearance of resonant dips and peaks in the spectrum of the scattered signal, which determine the characteristics of the scatterer. The described decrease in the width of the initial time window during processing reduces the actual frequency resolution, discarding some of the scattered weak signals, and therefore smooths out the real resonant features. Therefore, a time window was also introduced into the theoretical calculations, which was used in the experimental data processing, to approximate the results of theoretical calculations to the conditions in which the experimental curves were obtained.

For the selected part of a signal, the signal spectrum was calculated using the Fourier transform. The frequency range that was used for the analysis was limited to the frequencies at which the modulus of the spectral amplitude of the incident field decreased by a factor of 10 relative to the maximum of the given pulse.

Measurements along the  $y$  axis gave the angular distribution of the scattered-field amplitude; separately, a measurement at the central point of this distribution, which lay on the acoustic axis, was taken for the analysis in order to obtain the frequency dependence of the forward-scattering amplitude. When analyzing the scattering, it was revealed that the frequency dependence of the forward-scattering amplitude is more sensitive to changes in  $c_l$  and  $c_t$ , compared to the angular distribution; therefore, just this dependence was used to find the unknown velocities. In addition, the scattered-field minima are the characteristic features in the angular distribution; their positions are determined with a larger error because of a signal decay at these angles virtually to zero and an increase in the role of noise, which introduces errors in the determination of these minima.

The following functional was used to determine the velocities of longitudinal  $c_l$  and transverse  $c_t$  waves:

$$\chi^2(c_l, c_t) = \sum_{n=1}^N \left( \left| (P_s^{\text{exp}})_n \right| - \left| (P_s(c_l, c_t))_n \right| \right)^2. \quad (11)$$

Here,  $P_s^{\text{exp}}$  is the experimentally measured amplitude,  $P_s(c_l, c_t)$  is the amplitude numerically calculated using formula (8) (or formula (3) in the approximation of the incidence of a plane wave on the sphere),  $N$  is the number of different frequencies at which forward scattering was considered or the number of different spatial points, at which the angular distribution of the scattered field was measured. By varying the values of  $c_l$  and  $c_t$  and minimizing the functional (11), these velocities were determined. It is possible to consider other sets of arguments of the functional: e.g., the dependences on only one variable  $\chi^2(c_l)$ .

If the measurement results showed that the absorption played an appreciable role (in the case of nylon

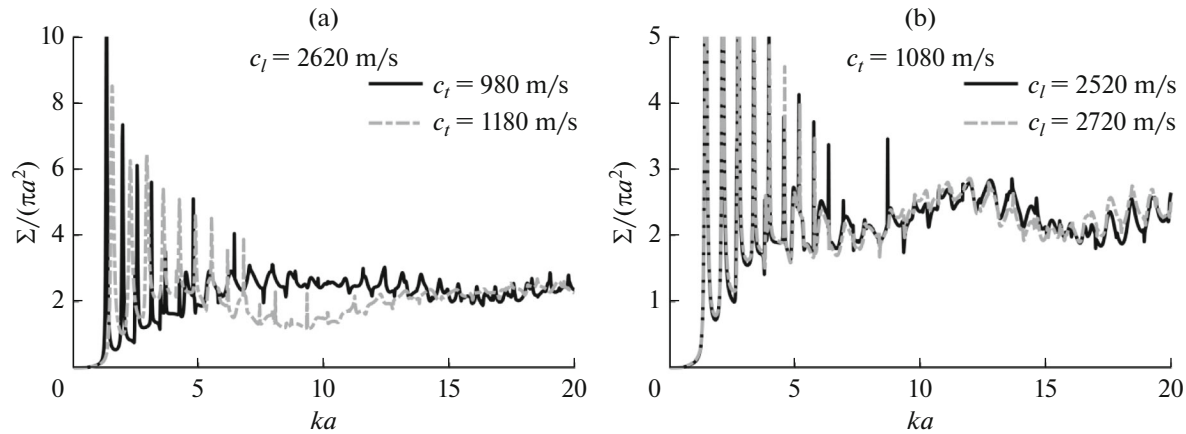


**Fig. 3.** Scattering cross-section normalized to cross-sectional area of sphere as function of dimensionless parameter  $ka$  with variations of velocities of (a) transverse  $c_t$  and (b) longitudinal waves  $c_l$  for nylon sphere.

spheres), the loss tangents, which were introduced according to formula (7), were preliminarily assessed by the degree of smoothness of the experimental dependence of the forward-scattering amplitude, taking into account that the absorption of longitudinal waves is much weaker than that of transverse waves.

The errors in the velocities of the found longitudinal and transverse waves due to the proposed method and some asphericity of the spheres were estimated.

For indirect verification of the obtained values, the results of experimental measurements on the  $y$  axis were compared to numerical calculations. The best match of the two curves occurred when substituting the above-determined velocities.

## 4. RESULTS

### 4.1. Analysis of the Influence of Various Parameters of Spheres on the Characteristics of the Scattered Field

The theoretical study of the influence of various parameters on the scattered field was performed by calculating the scattering cross-section for steel, glass, and nylon spheres that were used in the experiments. The study of the degree and nature of the influence of each of the parameters on the scattering cross-section was of interest. According to calculations, a change in the density of the sphere material by 5% (this value exceeds the maximum density-measurement error in this study) affects the cross-section so slightly that it can be considered independent of the sphere density within the permissible error. The effect of the velocity of sound in water on the scattering cross-section was more noticeable: the positions of the peaks and dips were shifted, and their shape and maximum values changed. For more accurate calculations, it is also important to measure the velocity of sound in water at the time of the experiments.

In contrast to the sphere density and the velocity of sound in water, the influence of the velocities of longi-

tudinal  $c_l$  and transverse  $c_t$  waves on the frequency dependence of the scattering cross-section was quite strong. Figure 3 shows the dependences of the normalized scattering cross-section on the dimensionless parameter  $ka$  under variations in the values of the transverse  $c_t$  (Fig. 3a) and longitudinal  $c_l$  velocities (Fig. 3b) for the nylon sphere. As is seen, the positions and shapes of the peaks and dips strongly depend on the values of the elastic velocities. However, at low frequencies, the resonances are mainly determined by transverse waves: variations in the velocity of longitudinal waves cause only small changes in the frequency and amplitude imperceptible in comparison with analogous changes introduced by variations in the velocity of transverse waves. A dependence of the scattering cross-section on the velocity of longitudinal waves appears at higher frequencies.

Similar frequency dependences can be constructed for the forward-scattering amplitude and qualitatively the same results can be obtained. Thus, in the frequency ranges that contain resonant peaks or dips, the scattered field is sensitive to small changes in the velocities of longitudinal and transverse waves. At the same time, the scattered field changes slightly under changes in the other parameters that determine scattering. This makes it possible to use the frequency or angular dependences of the scattered-field amplitude in these frequency ranges to determine the velocities of elastic waves.

Along with the wave velocities and density, the loss tangents for different types of waves in the scatterer are important parameters. Figure 4 shows the frequency dependences of the normalized scattering cross-section when nonzero loss tangents appear in the calculations. Since low-frequency resonances are mainly caused by transverse waves, no broadening of such a resonance occurs with an increase in the loss tangent of longitudinal waves. As the loss tangent of transverse waves  $\tan\delta_t$  increases, the resonance amplitude

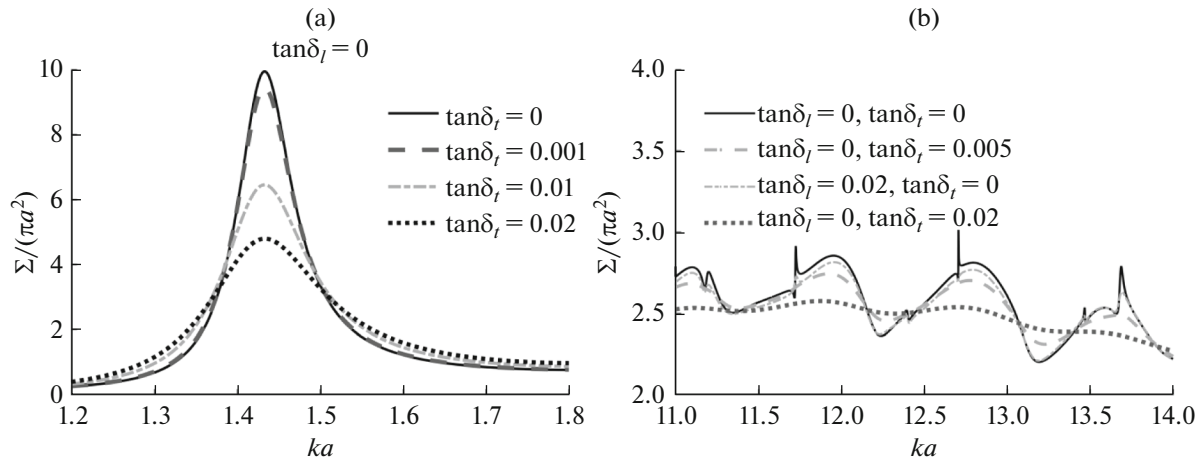


**Fig. 4.** Scattering cross-section normalized to cross-sectional area of sphere as function of parameter  $ka$  under variations of loss tangents for longitudinal waves  $\tan \delta_l$  and transverse waves  $\tan \delta_t$  in various  $ka$  ranges.

decreases and the width increases (Fig. 4a). Thus, the resonance curve caused by transverse waves broadens when the effect of transverse-wave absorption occurs in the scatterer material. High-frequency resonances are caused by both types of elastic waves; however, the degree of dependence on the transverse-wave velocity is still greater. Figure 4b shows the smoothing of the resonances with an increase in the loss tangent of both longitudinal and transverse waves. The dependence of the resonances mainly on the transverse wave velocity manifests itself in a stronger broadening of the resonances with increasing  $\tan \delta_t$ . The broadening of the resonance curves also occurs with increasing  $\tan \delta_l$  but much more slowly. Thus, the main contribution of accounting the absorption is that the resonance curves become smoother, while at some frequencies, e.g., between the resonant peaks, the amplitude may even increase in comparison to the case without absorption.

#### 4.2. Determination of Unknown Parameters of Solid Spheres Based on Experimental Investigation of the Scattering Characteristics

**4.2.1. Investigation of the properties of steel spheres.** The experiments were carried out for three steel spheres of different sizes (see Table 1). The sound absorption in steel at the considered frequencies is low and can be neglected. The smallest of the steel spheres presented has a diameter of 2.8 mm. It was found that the discrepancy between the amplitudes of the scattered field calculated at the considered frequencies for the cases of an ultrasound beam and a plane wave incident on this sphere is less than 1%. Therefore, to determine the unknown parameters of the scatterer, it is sufficient to use the plane-wave approximation.

When calculating the scattering for this sphere in the megahertz frequency range, resonances sensitive to the velocity of the longitudinal waves are not

detected. Therefore, only the transverse-wave velocity can be determined in this frequency range. By comparing the experimental frequency dependence of the forward-scattering amplitude with that numerically calculated from formula (3) and minimizing the sum of the squared deviations of the points of these dependences from one another by varying the transverse wave velocity  $c_t$  at  $c_l = \text{const}$  (Fig. 5a), the unknown velocity  $c_t = 3340 \pm 15$  m/s was determined. Figure 5b shows the experimental dependence of the forward-scattering amplitude, as well as the numerically calculated dependences for three transverse-wave velocities, one of which ( $c_t = 3340$  m/s) approximates well the numerical calculations to the experimental dependence. The lack of smoothness in the experimental dependence may be due to the occurrence of rereflected signals between the sphere and the hydrophone in the recorded signal due to the small distance between them, which had to be used to reduce the influence of noise, since the scattering from a small object is weak, and the scattered field rapidly decreases with the distance from the scatterer.

Since a drop of the incident field at the edges of the sphere becomes noticeable for steel spheres with diameters of 4.75 and 6 mm, the numerical calculation should be performed taking the spatial structure of the beam into account. The complex amplitude of the acoustic pressure created by the source in the transverse plane, which runs through the center of the sphere, was calculated using the Rayleigh integral. Subsequently, using two-dimensional Fourier transform (9), the angular spectrum  $S(k_x, k_y)$  was found, which is used in the calculations of the scattering-determining coefficients.

For a steel sphere with a diameter of 4.75 mm, the situation is similar to that considered above: in the selected frequency range, the scattering cross-section

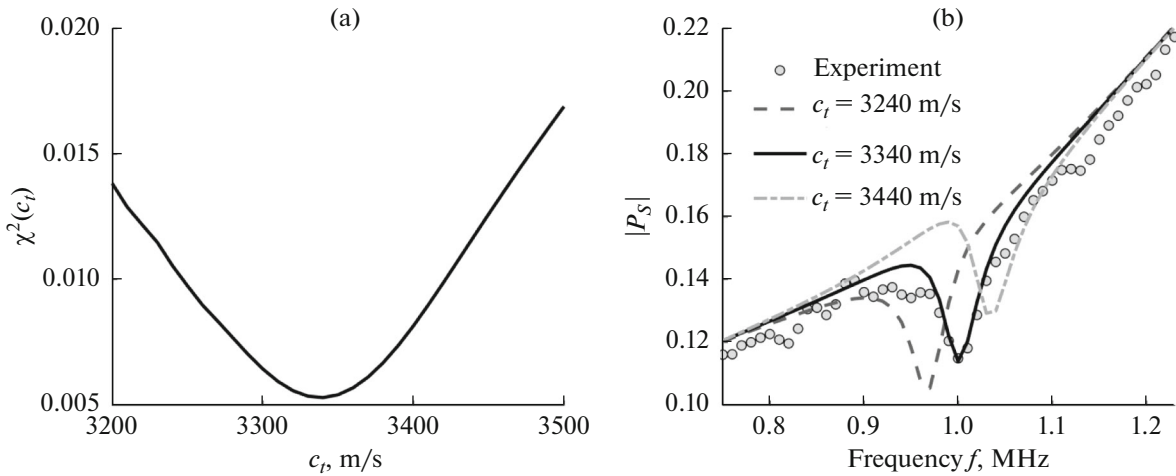


**Fig. 5.** Results for steel sphere with diameter of 2.8 mm. (a) Sum of squared deviations between points of experimental and numerically calculated frequency dependences of forward-scattering amplitudes as function of velocity of transverse waves  $\chi^2(c_t)$ . Minimum in this dependence corresponds to desired velocity of transverse waves in scatterer. (b) Frequency dependence of forward-scattering amplitude (points) experimentally measured values and (solid curves) numerically calculated values for indicated velocities of transverse waves  $c_t$ . Scattered-wave amplitude is normalized to incident-field amplitude at the center of the sphere.

almost does not change when the velocity of longitudinal waves changes within the permissible values; as a result, only the velocity of transverse waves can be determined (see Table 2). The results of experimental measurements and numerical calculations are shown in Fig. 6 (upper row).

The weak dependence of the scattering cross-section on  $c_t$  indicates a weak influence of this physical quantity on the scattering in the given frequency range for this sphere. Thus, it can be assumed that all the parameters that determine the character of scattering and related phenomena have been determined.

The scattering cross-section of a steel sphere with a diameter of 6 mm in the megahertz frequency range depends on the velocities of both longitudinal and transverse waves; therefore, both velocities can be determined from the results of scattered-field measurements. By varying the velocities of longitudinal and transverse waves (Fig. 6d) and minimizing the departure of the experimental frequency dependence of the forward-scattering amplitude on the numerically calculated one, the velocities of the longitudinal and transverse waves were determined (see Fig. 6, lower part, and Table 2).

The results of the experimental measurements were compared to the numerical calculations for the found elastic velocities. Figures 6b and 6e show the experimental and numerically calculated curves that correspond to the frequency dependences of the forward-scattering amplitude, for which the minimization was performed. Figures 6c and 6f show the results of the experimental measurements on the y axis and numerical calculations; no minimization for these experimental points was performed because of the lower sensitivity of the axial distribution to changes in the elastic velocities.

For the velocities  $c_t$  that could not be determined because of the weak dependence of the scattered field on them, the values that were specified by the manufacturer were used for calculations, and variations of the velocity values within the limits of the reference data (Table 2) did not influence the calculation results.

It should be noted that the frequency ranges within which scattering depends only on the velocity  $c_t$  of transverse waves can be initially selected for rigid materials, and proceeding from the experimental data,  $c_t$  in this region can be determined. Measurements can then be performed in the frequency region where there

**Table 2.** Determination of parameters of steel spheres

Experimental results				Reference data [36, 37]
diameter $d$ , mm	designation, mm	$c_t$ , m/s	$c_l$ , m/s	
$2.763 \pm 0.005$	2.8	$3340 \pm 15$	—	$c_t = 3180\text{--}3340$ m/s $c_l = 5680\text{--}6100$ m/s
$4.744 \pm 0.005$	4.75	$3190 \pm 15$	—	
$5.989 \pm 0.005$	6	$3245 \pm 10$	$5930 \pm 50$	

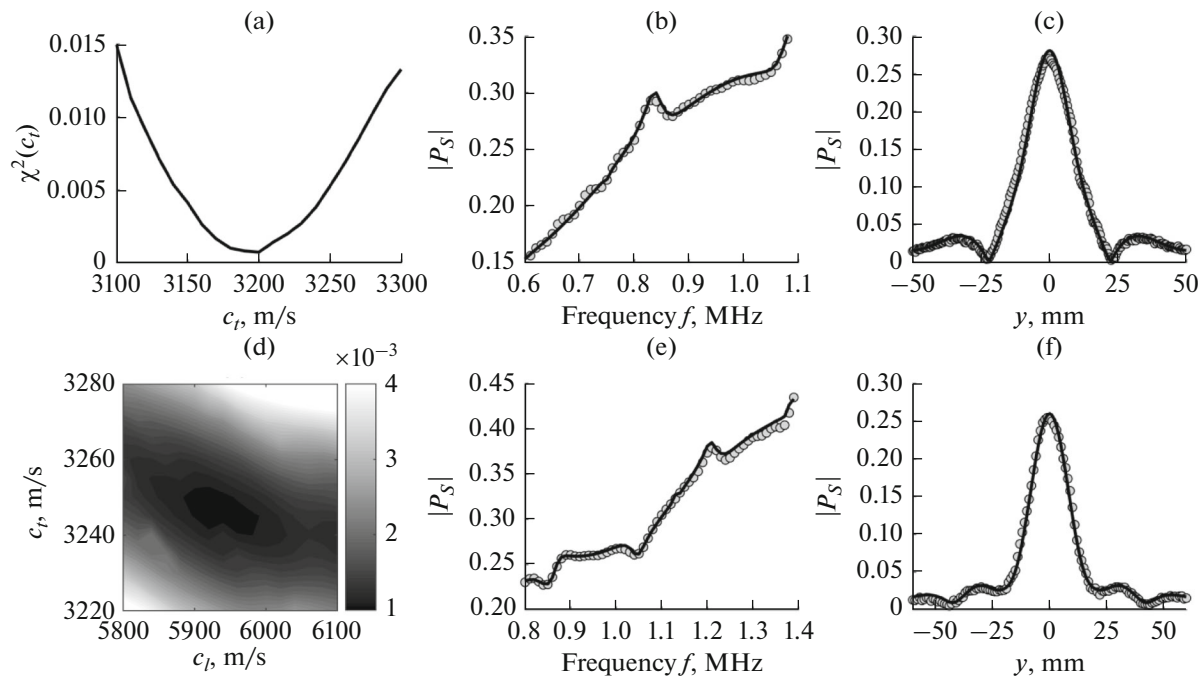


**Fig. 6.** Results for steel spheres with diameters of 4.75 (upper row) and 6 mm (bottom row). Sum of squared deviations of points between experimental and numerically calculated frequency dependences of forward-scattering amplitudes for (a) sphere with diameter of 4.75 mm as function of velocities  $c_t$  of transverse waves  $\chi^2(c_t)$  and (d) sphere with diameter of 6 mm as function of velocities of transverse  $c_t$  and longitudinal  $c_l$  waves  $\chi^2(c_t, c_l)$ ; (b, e) frequency dependence of forward-scattering amplitude; (c, f) amplitude of scattered field as function of  $y$  coordinate at frequencies of 0.83 (top) and 1.04 MHz (bottom). Points are experimentally measured values; curves were numerically calculated for found velocities  $c_t$  and  $c_l$  (given in Table 2). Scattered-wave amplitude is normalized to incident-field amplitude at the center of the sphere.

is a dependence on the velocity  $c_l$  of longitudinal waves, and knowledge of the velocity  $c_t$ , which is determined from the previous operation, allows finding  $c_l$ .

**4.2.2. Investigation of the properties of glass spheres.** In the case of glass spheres, the scattering analysis did not reveal noticeable sound-absorption effects in the sphere material; therefore, the method described above for steel spheres was used, taking the spatial structure of the beam into account. The determined velocities are presented in Table 3. The results of measurements and numerical calculations are shown in Fig. 7.

Since the value of the scattered field in this frequency range depends more on the velocity of transverse waves, the error in their determination is much

lower than for the velocity of longitudinal waves. For a sphere with a diameter of 6.1 mm, the  $c_l$  value could not be determined because of its weak effect on the form of the scattered field (the second line in Fig. 7), while for the other two spheres,  $c_l$  is determined with a large error.

**4.2.3. Investigation of the properties of nylon spheres.** Unlike steel and glass spheres, in which the sound absorption is so small that it can be disregarded, the presence of absorption in nylon spheres significantly and strongly modifies the scattered field; therefore, it must be taken into account in the calculations. Experiments were performed with nylon spheres with diameters of 4, 6, and 8 mm to assess the absorption effect.

**Table 3.** Determination of parameters of glass spheres

Experimental results				Reference data [36–38]
diameter $d$ , mm	designation, mm	$c_t$ , m/s	$c_l$ , m/s	
$3.967 \pm 0.006$	4	$3300 \pm 15$	$5950 \pm 50$	$c_t = 3400\text{--}3740$ m/s $c_l = 5570\text{--}6000$ m/s
$6.104 \pm 0.019$	6.1	$3420 \pm 30$	—	
$7.981 \pm 0.006$	8	$3425 \pm 15$	$5740 \pm 100$	

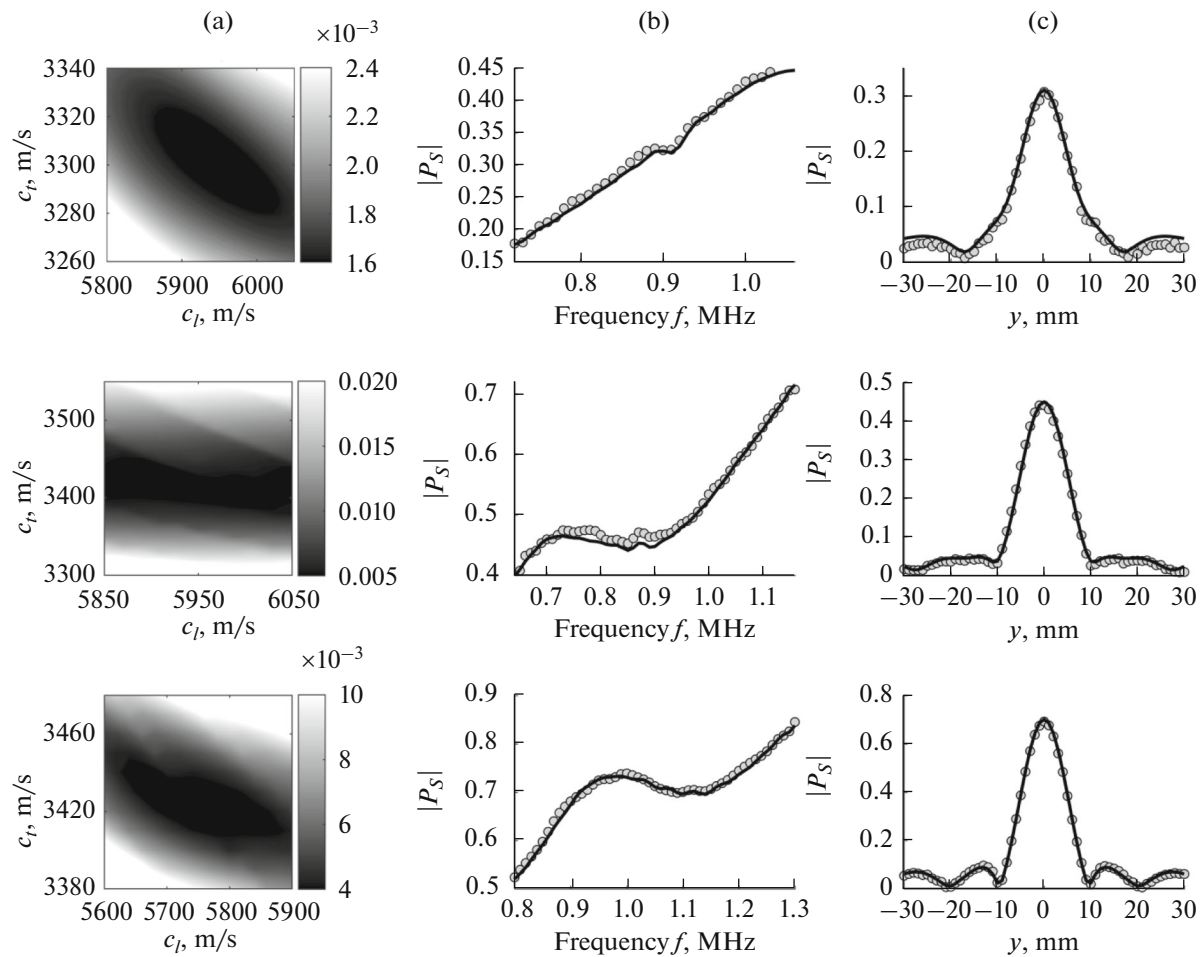


**Fig. 7.** Results for glass spheres with diameters of 4, 6.1, and 8 mm (downward). (a) Sum of squared deviations of points between experimental and numerically calculated frequency dependences of forward-scattering amplitudes as function of velocities of transverse  $c_t$  and longitudinal  $c_l$  waves ( $\chi^2(c_l, c_t)$ ); (b) frequency dependence of forward-scattering amplitude; (c) scattered-field amplitude as function of  $y$  coordinate at frequencies of 0.91, 0.9, and 1.1 MHz (downwards). Points are experimentally measured values; curves correspond to numerically calculated values for found velocities  $c_t$  and  $c_l$  (see Table 3). Scattered-wave amplitude is normalized to incident-field amplitude at the center of the sphere.

Good results were achieved in an experiment with a 4-mm-diameter sphere. The loss tangents that were introduced according to formula (7) were preliminarily evaluated by the degree of smoothness of the experimental dependence of the forward-scattering amplitude. Subsequently, using the obtained approximate values of the loss tangents, the elastic wave velocities were determined by minimizing the deviation of the experimental frequency dependence of the forward-scattering amplitude from the corresponding theoretical dependence. After that, the loss tangents of the transverse and longitudinal waves were refined. It is known that longitudinal waves in nylon are absorbed to a much smaller degree than transverse waves. However, the resonances in nylon depend on the transverse-wave velocity to a higher degree. As a result, the accuracy of determining the loss tangent of longitudinal waves is much lower, but the determined value

itself is an order of magnitude smaller and also has a weak effect on scattering. These results are shown in Fig. 8, and the found values are listed in Table 4.

During similar processing of the experimental results for nylon spheres with diameters of 6 and 8 mm, no set of elastic wave velocities was observed at which the calculated curves of the frequency dependences of the forward-scattering amplitudes would approach the experimental curves. This mismatch of the curves can be caused either by defects or inhomogeneities in the sphere material, or by the uncertainty of its parameters, which depend on the manufacturing process. To exclude cases of single defects in the material, experiments were performed with several spheres with 6-mm diameters. The results for two of them are presented. It was noticed that in some frequency ranges, the numerically calculated frequency depen-

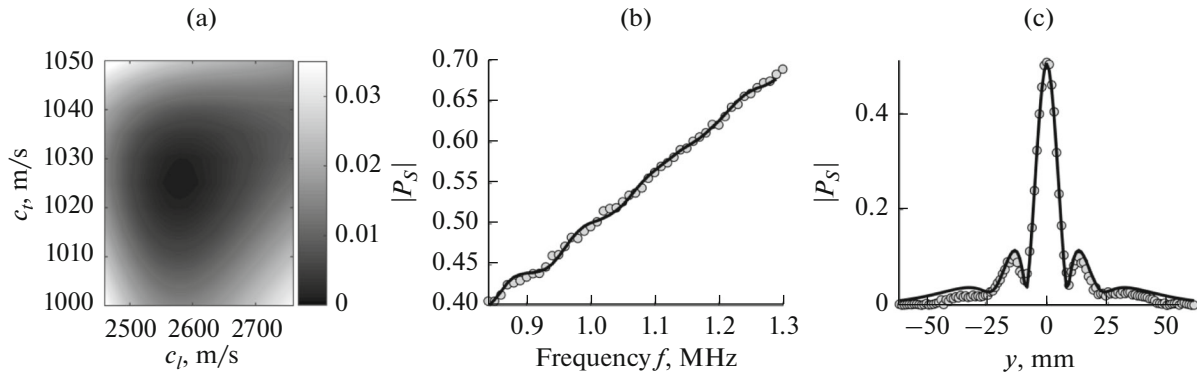


**Fig. 8.** Results for nylon sphere with diameter of 4 mm. (a) Sum of squared deviations of points between experimental and numerically calculated frequency dependences of forward-scattering amplitudes as function of velocities of transverse  $c_t$  and longitudinal  $c_l$  waves ( $\chi^2(c_t, c_l)$ ); (b) frequency dependence of forward-scattering amplitude; (c) scattered-field amplitude as function of  $y$  coordinate at frequency of 1 MHz. Points are experimentally measured values; solid curves correspond to numerically calculated values for found velocities  $c_t$  and  $c_l$  (see Table 4). Scattered-wave amplitude is normalized to incident-field amplitude at the center of the sphere.

dences of the forward-scattering amplitude overlap with the experimental dependences in the vicinity of some of the  $c_t$  and  $c_l$  values indicated on the graphs (see Fig. 9b). In view of this, the distribution of the scattered field along the  $y$  axis was taken for analysis at these frequencies, and by minimizing the sum of the squared deviations between the points of the experimentally obtained and calculated angular dependences with varying values of  $c_t$  and  $c_l$ , the unknown velocities were determined (see Figs. 9a, 9c and Table 4).

As a result of the above measurements for the nylon sphere, several parameters were determined: the velocities of the longitudinal and transverse waves and the loss tangents. This can be done because different parameters have qualitatively different effects on scattering, and the other physical quantities that determine scattering are known with the necessary accuracy. Different contributions to the scattered field from different parameters also lead to different relative errors in determining these parameters.

Thus, the velocities of the longitudinal and transverse waves were refined for the scatterers, and the loss

tangents of the longitudinal and transverse waves were estimated as well. The obtained values lie in the range of the tabular velocity values for these materials.

## 5. CONCLUSIONS

Studying phenomena related to the effect of the acoustic field on scatterers requires knowledge of the scatterer characteristics with the highest possible accuracy. The elastic constants of the scatterers available for experiments are not always precisely known, since their values may vary depending on the production process. As a result, the elastic parameters of a sphere, i.e., the velocities of longitudinal and transverse waves, are known with a large error and there are no simple ways to determine these parameters.

Our study has demonstrated that experimental measurements of the scattered field, namely, the frequency dependences of the forward-scattering amplitudes and the angular distribution, can be used to determine the velocities of longitudinal and transverse waves and estimate the absorption in elastic spherical scatterers of millimeter size.

**Table 4.** Determination of parameters of nylon spheres

Experimental results					
diameter $d$ , mm	designation, mm	$c_t$ , m/s	$c_l$ , m/s	$\tan \delta_t$	$\tan \delta_l$
$3.945 \pm 0.005$	4	$1025 \pm 5$	$2580 \pm 25$	$0.025 \pm 0.002$	$\sim 0.005 \pm 0.005$
$5.930 \pm 0.007$	6	$1100 \pm 15$	$2510 \pm 40$	$0.020 \pm 0.005$	—
$5.958 \pm 0.007$	6	$1120 \pm 15$	$2550 \pm 30$	$0.020 \pm 0.005$	—
$7.990 \pm 0.007$	8	$1100 \pm 15$	$2700 \pm 50$	$0.020 \pm 0.005$	—
Reference data [36–39]					
$c_t = 900\text{--}1100$ m/s			$c_l = 1800\text{--}2650$ m/s		

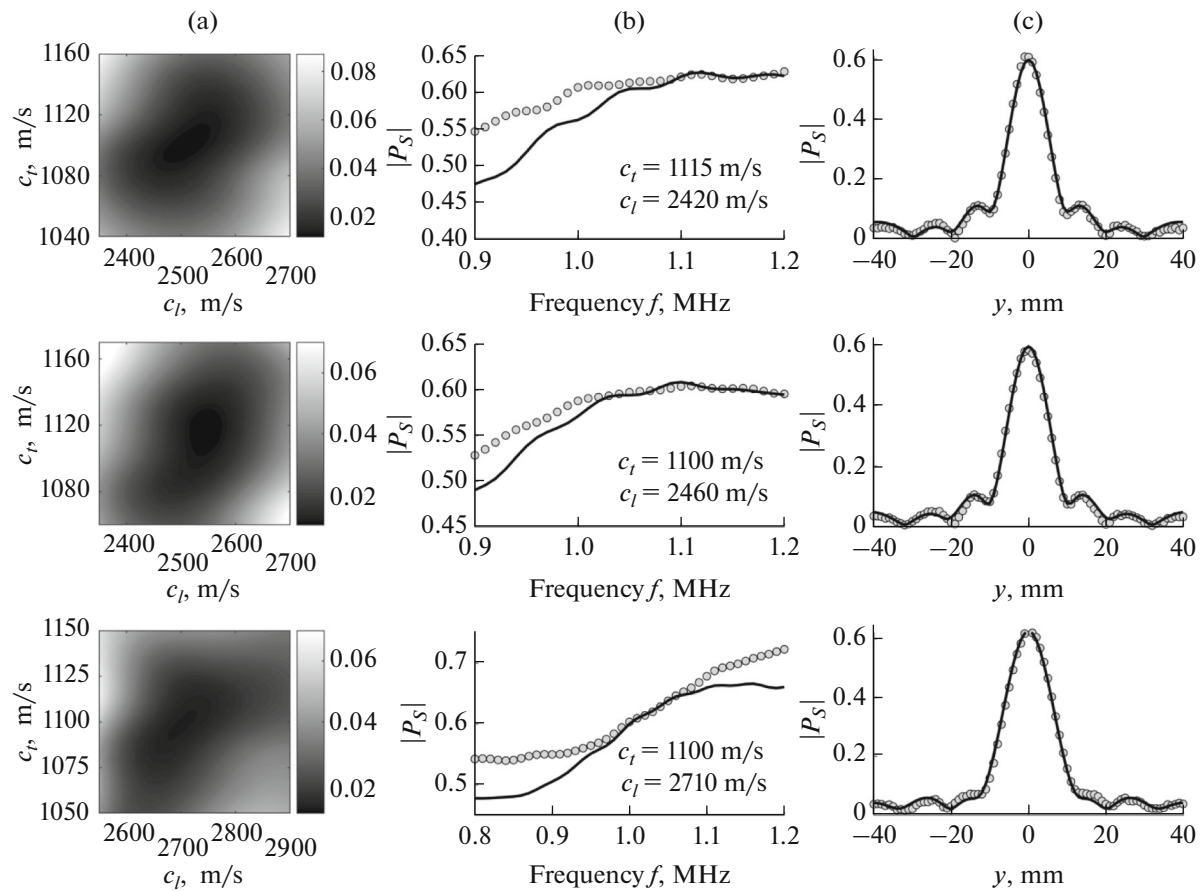


**Fig. 9.** Results for nylon spheres with diameters of 6 (two upper rows) and 8 mm (bottom row). (a) Sum of squared deviations of points between experimental and numerically calculated angular dependences of forward-scattering amplitudes as function of velocities of transverse  $c_t$  and longitudinal  $c_l$  at frequencies of 1.12 and 1.1 MHz for spheres with diameter of 6 mm, and 1.05 MHz for sphere with diameter of 8 mm (downwards) ( $\chi^2(c_t, c_l)$ ); (b) frequency dependence of forward-scattering amplitude; (c) scattered-field amplitude as function of  $y$  coordinate at same frequencies. Points are experimentally measured values; solid curves were calculated numerically: (b) for  $c_t$  and  $c_l$  values indicated on graphs, (c) for found  $c_t$  and  $c_l$  values (see Table 4). Scattered-wave amplitude is normalized to incident-field amplitude at the center of the sphere.

An experimental setup for observing scattering by spheres of millimeter dimensions, which does not introduce distortions into the scattered field, has been created. Experiments with steel, glass, and nylon spheres with diameters of 2.8–8 mm were performed. The spatial beam structure was taken into account in the scattered-field calculations, thus significantly improving the coincidence of the experimental and theoretical curves. Using the developed technique, the velocities of longitudinal and elastic waves in scatterers were refined, and the loss tangents in the case of nylon spheres were estimated. The obtained values are in the range of tabulated values for these materials.

Based on the experimental measurement results, it was found that absorption in steel and glass spheres is negligible and does not affect scattering, while in nylon spheres, transverse waves are absorbed intensely, and this must be taken into account when

matching the theoretical calculations to the experimental data.

The found errors of the obtained values of the elastic wave velocities are in the range of 0.3–1.9%. The error of the method can be reduced by increasing the frequency resolution to register narrower peaks, which are more sensitive to the values of the elastic velocities, and to determine the velocities by several resonance features by investigating several different frequency ranges.

#### FUNDING

This study was supported by the Russian Science Foundation, project no. 19-12-00148. The theoretical part of this study was performed with the support of a grant from the Theoretical Physics and Mathematics Advancement Foundation “BASIS” (L.M. Kotelnikova).

## REFERENCES

1. V. A. Krasil'nikov and V. V. Krylov, *Introduction to Physical Acoustics* (Nauka, Moscow, 1984) [in Russian].
2. K. N. Rozhdestvenskii and L. A. Tolokonnikov, *Akust. Zh.* **36** (5), 927 (1990).
3. E. L. Shenderov, *Acoust. Phys.* **48** (5), 607 (2002).
4. S. M. Hasheminejad and M. Maleki, *Acoust. Phys.* **54** (2), 168 (2008).
5. V. A. Bulanov and L. Bjorno, *Akust. Zh.* **38** (2), 252 (1992).
6. A. V. Nikolaeva, S. A. Tsysar, and O. A. Sapozhnikov, *Acoust. Phys.* **62** (1), 38 (2016).
7. L. A. Mal'tseva, M. A. Gervas'ev, and A. B. Kut'in, *Material Science* (Ural Federal Univ., Yekaterinburg, 2012) [in Russian].
8. D. N. MacLennan and J. R. Dunn, *J. Sound Vib.* **97** (2), 321 (1984).
9. J. J. Faran, *J. Acoust. Soc. Am.* **23** (4), 405 (1951).
10. R. Hickling, *J. Acoust. Soc. Am.* **34** (10), 1582 (1962).
11. L. Flax and H. Überall, *J. Acoust. Soc. Am.* **67** (5), 1432 (1980).
12. H. Überall, *Trait. Signal* **2** (5), 353 (1985).
13. G. C. Gaunaurd and H. Überall, *J. Acoust. Soc. Am.* **73** (1), 1 (1983).
14. G. C. Gaunaurd, *IEEE J. Oceanic Eng.* **12** (2), 419 (1987).
15. L. Flax, L. R. Dragonette, and H. Überall, *J. Acoust. Soc. Am.* **63** (2), 723 (1978).
16. J. W. S. Rayleigh, *Theory of Sound* (Macmillan, 1894; Gostekhteorizdat, Moscow, 1955), Vol. 2.
17. J. W. Strutt, *Philos. Mag.* **20** (120), 1001 (1910).
18. R. H. Vogt and W. G. Neubauer, *J. Acoust. Soc. Am.* **60** (1), 15 (1976).
19. J. P. Sessarego, J. Sageloli, R. Guillermin, and H. Überall, *J. Acoust. Soc. Am.* **104** (5), 2836 (1998).
20. G. C. Gaunaurd and M. F. Werby, *J. Acoust. Soc. Am.* **89** (6), 2731 (1991).
21. E. L. Shenderov, *Sound Radiation and Scattering* (Sudostroenie, Leningrad, 1989) [in Russian].
22. K. L. Williams and P. L. Marston, *J. Acoust. Soc. Am.* **78** (3), 1093 (1985).
23. K. G. Foote, in *Proc. IEEE Ultrasonics Symp.* (Chicago, Oct. 14–16, 1981).
24. H. Hobæk and T. N. Forland, *Acta Acust. Acust.* **99** (3), 465 (2013).
25. W. G. Neubauer, R. H. Vogt, and L. R. Dragonette, *J. Acoust. Soc. Am.* **55** (6), 1123 (1974).
26. L. R. Dragonette, R. H. Vogt, L. Flax, and W. G. Neubauer, *J. Acoust. Soc. Am.* **55** (6), 1130 (1974).
27. V. M. Ayres and G. C. Gaunaurd, *J. Acoust. Soc. Am.* **82** (4), 1291 (1987).
28. J. M. Perdigão, A. Ferreira, J. E. Lefebvre, and C. Bruneel, *Ultrasonics* **26** (2), 102 (1988).
29. S. A. Tsysar, V. A. Khokhlova, and W. Kreider, *J. Acoust. Soc. Am.* **138** (3), 1515 (2015).
30. O. A. Sapozhnikov and M. R. Bailey, *J. Acoust. Soc. Am.* **133** (2), 661 (2013).
31. P. M. Morse and H. Feshbach, *Methods of Theoretical Physics* (McGraw-Hill, New York, 1953; Inostrannaya literatura, Moscow, 1959), Vol. 2.
32. W. J. Wiscombe, *Appl. Opt.* **19** (9), 1505 (1980).
33. H. C. Strifors and G. C. Gaunaurd, *J. Acoust. Soc. Am.* **85** (3), 995 (1989).
34. R. H. Vogt, L. Flax, L. R. Dragonette, and W. G. Neubauer, *J. Acoust. Soc. Am.* **57** (3), 558 (1975).
35. V. M. Ayres and G. C. Gaunaurd, *J. Acoust. Soc. Am.* **81** (2), 301 (1987).
36. A. R. Selfridge, *IEEE Trans. Sonics Ultrason.* **32** (3), 381 (1985).
37. *Physical Quantities: Handbook*, Ed. by I. S. Grigor'ev and E. Z. Meilikhov (Energoatomizdat, Moscow, 1991) [in Russian].
38. I. K. Kikoin, *Tables of Physical Quantities* (Atomizdat, Moscow, 1976) [in Russian].
39. N. A. Kozlov and A. D. Mitrofanov, *Polymers Physics* (Vladimir State Univ., Vladimir, 2001) [in Russian].

*Translated by A. Seferov*